

See discussions, stats, and author profiles for this publication at: <https://www.researchgate.net/publication/325551831>

# Electron microprobe technique for the determination of iron oxidation state in silicate glasses

Article in *American Mineralogist* · June 2018

DOI: 10.2138/am-2018-6437

CITATIONS

2

READS

443

8 authors, including:



**Chao Zhang**

Northwest University

66 PUBLICATIONS 619 CITATIONS

[SEE PROFILE](#)



**Renat R. Almeev**

Leibniz Universität Hannover

80 PUBLICATIONS 1,188 CITATIONS

[SEE PROFILE](#)



**Ery Hughes**

California Institute of Technology

10 PUBLICATIONS 17 CITATIONS

[SEE PROFILE](#)



**Alexander Borisov**

Russian Academy of Sciences

97 PUBLICATIONS 1,696 CITATIONS

[SEE PROFILE](#)

Some of the authors of this publication are also working on these related projects:



Okataina Volcanic Centre [View project](#)



EPMA of silicate glass [View project](#)

## Electron microprobe technique for the determination of iron oxidation state in silicate glasses

CHAO ZHANG<sup>1</sup>, RENAT R. ALMEEV<sup>1,\*</sup>, ERY C. HUGHES<sup>2</sup>, ALEXANDER A. BORISOV<sup>3</sup>, ERIC P. WOLFF<sup>1</sup>, HEIDI E. HÖFER<sup>4</sup>, ROMAN E. BOTCHARNIKOV<sup>5</sup>, AND JÜRGEN KOEPKE<sup>1</sup>

<sup>1</sup>Leibniz Universität Hannover, Institut für Mineralogie, Callinstrasse 3, D-30167, Hannover, Germany

<sup>2</sup>School of Earth Sciences, University of Bristol, Bristol BS8 1RJ, U.K.

<sup>3</sup>Institute of Geology of Ore Deposits, Petrography, Mineralogy, and Geochemistry, Russian Academy of Sciences, Staromonetny 35, 109017 Moscow, Russia

<sup>4</sup>Institut für Geowissenschaften, Mineralogie, Johann Wolfgang Goethe-Universität, Altenhöferallee 1, D-60438 Frankfurt am Main, Germany

<sup>5</sup>Institute für Geowissenschaften, Johannes Gutenberg Universität Mainz, J-J-Becher-Weg 21, D-55128 Mainz, Germany

### ABSTRACT

We present a new calibration for the determination of the iron oxidation state in silicate glasses by electron probe microanalysis (EPMA) with the “flank method.” This method is based on the changes in both intensity and wavelength of the FeL $\alpha$  and FeL $\beta$  X-ray emission lines with iron oxidation state. The flank method utilizes the maximum difference for the FeL $\alpha$  and FeL $\beta$  spectra observed at the peak flanks between different standard materials, which quantitatively correlates with the Fe<sup>2+</sup> content. Provided that this correlation is calibrated on reference materials, the Fe<sup>2+</sup>/ $\Sigma$ Fe ratio can be determined for samples with known total Fe content. Two synthetic Fe-rich ferric and ferrous garnet end-members, i.e., andradite and almandine, were used to identify the FeL $\alpha$  and FeL $\beta$  flank method measuring positions that were then applied to the measurement of a variety of silicate glasses with known Fe<sup>2+</sup>/ $\Sigma$ Fe ratio (ranging from 0.2 to 1.0). The measured intensity ratio of FeL $\beta$  over FeL $\alpha$  at these flank positions (L $\beta$ /L $\alpha$ ) is a linear function of the Fe<sup>2+</sup> content (in wt%). A single linear trend can be established for both garnets and silicate glasses with 4–18 wt% FeO<sub>T</sub> (total iron expressed as FeO). In glasses with up to 18 wt% FeO<sub>T</sub> and 15 wt% TiO<sub>2</sub>, no systematic compositional (matrix) effects were observed. A possible influence of Ti on the Fe<sup>2+</sup> determination has only been observed in one high-Ti glass with ~25 wt% TiO<sub>2</sub>, a content that is not typical for natural terrestrial silicate melts. The accuracy of the Fe<sup>2+</sup>/ $\Sigma$ Fe determination, which depends on both the Fe<sup>2+</sup> content determined with the flank method and on the total Fe content, is estimated to be within  $\pm 0.1$  for silicate glasses with FeO<sub>T</sub> > 5 wt% and within  $\pm 0.3$  for silicate glasses with low FeO<sub>T</sub>  $\leq$  5 wt%. The application of the flank method on silicate glasses requires minimization of the EPMA beam damage that can be successfully achieved by continuous movement of the sample stage under the electron beam during analysis, e.g., with a speed of 2  $\mu$ m/s.

**Keywords:** Microprobe, ferric-ferrous ratio, silicate glasses, redox state, flank method, pillow glasses

### INTRODUCTION

Fe is the most abundant transition metal in magmatic systems of the Earth. Depending on the redox condition, Fe can be present in different oxidation states (Fe<sup>3+</sup>, Fe<sup>2+</sup>, and Fe<sup>0</sup>). The oxidation state of Fe in natural silicate glasses is an important parameter that reflects the redox conditions prevailing during magma generation and/or crystallization (e.g., Christie et al. 1986; Bézos and Humler 2005; Cottrell and Kelley 2011; Kelley and Cottrell 2009). It varies as a complex function of oxygen fugacity, temperature, pressure, and melt composition (e.g., Sack et al. 1981; Borisov and Shapkin 1990; Kress and Carmichael 1991; Nikolaev et al. 1996; Moretti 2005; Schuessler et al. 2008; Borisov et al. 2015). Due to the influence of ferrous and ferric Fe on the local structure of silicate melt, the oxidation state of Fe can significantly influence physical and chemical properties of silicate melts (e.g., viscosity, density, heat capacity, degree of polymerization and phase equilibrium, see review by Wilke 2005).

Both bulk and in situ techniques are available to determine the oxidation state of Fe in geological samples, which is usually expressed as Fe<sup>2+</sup>/ $\Sigma$ Fe or Fe<sup>3+</sup>/ $\Sigma$ Fe. The wet-chemistry colorimetric method of Wilson (1960) has been used as the most popular bulk analytical method providing a high accuracy (e.g., Schuessler et al. 2008). For the purpose of non-destructive and/or local high-resolution analysis, several in situ techniques have been developed, such as micro-Mössbauer spectroscopy (McCammon et al. 1991; Potapkin et al. 2012), X-ray absorption near edge structure (XANES) spectroscopy (Wilke et al. 2002), electron energy loss spectroscopy (EELS) (van Aken et al. 1998; van Aken and Liebscher 2002), and micro-Raman spectroscopy (Di Muro et al. 2009). Electron probe microanalysis (EPMA) has also been utilized to determine the Fe<sup>2+</sup>/ $\Sigma$ Fe ratio in geological samples, such as iron oxides (Höfer et al. 2000), garnets (Höfer and Brey 2007), olivines (Ejima et al. 2011), amphiboles (Enders et al. 2000; Lamb et al. 2012), and silicate glasses (Fialin et al. 2001, 2004, 2011). Despite methodological challenges observed so far, such as low sensitivity in some analytical protocols and lack

\* E-mail: r.almeev@mineralogie.uni-hannover.de

of standard materials, the easy access and low costs of EPMA compared to other methods keep it as a promising routine method for measuring the oxidation state of iron in various geological samples including silicate glasses.

In this paper, we present a new analytical technique for measuring the Fe oxidation state of silicate glasses with the EPMA flank method (Höfer and Brey 2007). Our tests performed on several silicate glasses show that the method can provide a determination of  $\text{Fe}^{2+}/\Sigma\text{Fe}$  with an accuracy of  $\pm 0.1$  for glasses containing 5–18 wt%  $\text{FeO}_T$ , and up to  $\pm 0.3$  for glasses containing  $\text{FeO}_T \leq 5$  wt%.

### THE FLANK METHOD

The application of EPMA to determine the oxidation state of Fe is based on the peak shift and energy difference of the  $\text{FeL}\alpha$  and  $\text{FeL}\beta$  emission lines for divalent and trivalent iron, which are induced by different electron energies of different bonding associated with  $\text{Fe}^{2+}$  and  $\text{Fe}^{3+}$  and their different self-absorption (see details in Fischer 1965; Tossell et al. 1974; Höfer et al. 1994). Changing from  $\text{Fe}^{2+}$  to  $\text{Fe}^{3+}$ , the  $\text{FeL}\alpha$  and  $\text{FeL}\beta$  lines are both shifted to a higher energy, and the intensity of  $\text{L}\beta$  peak is reduced preferentially to the  $\text{L}\alpha$  peak (Höfer et al. 1994). To date, two quantification techniques have been proposed: the “peak-shift method” and the “flank method.”

The *peak-shift method* utilizes the correlation between the peak positions of the  $\text{FeL}\alpha$  line and  $\text{Fe}^{3+}/\Sigma\text{Fe}$  ratio (Kimura and Akasaka 1999; Fialin et al. 2001, 2004, 2011). The peak-shift method requires accurate peak searches of the  $\text{FeL}\alpha$  line for all materials under investigation (both standards and unknowns), and may have large uncertainties for samples with low total Fe. This method does not consider the changes in intensity between the  $\text{FeL}\alpha$  and  $\text{FeL}\beta$  emission lines.

The *flank method* exploits both the peak shift and the intensity change of the  $\text{FeL}\alpha$  and  $\text{FeL}\beta$  lines with ferric iron content by measuring the intensities at specific positions on the flanks of  $\text{FeL}\alpha$  and  $\text{FeL}\beta$  peaks, respectively. Therefore, the flank method demonstrates higher sensitivity and better accuracy when compared to the peak-shift method (Höfer et al. 1994; Höfer and Brey 2007). So far, no application of the EPMA flank method for silicate glasses has been reported in the literature.

For the flank method, the optimal  $\text{FeL}\alpha$  flank and  $\text{FeL}\beta$  flank positions can be determined by the difference spectrum for a pair of materials with similar crystal structure and/or Fe coordination polyhedra but contrasting Fe oxidation states, such as wüstite-hematite (Höfer et al. 1994, 2000) and andradite-almandine (Fig. 1; Höfer 2002; Höfer and Brey 2007). The andradite ( $\text{Ca}_3^{2+}\text{Fe}_2^{3+}\text{Si}_3\text{O}_{12}$ ) and almandine ( $\text{Fe}_3^{2+}\text{Al}_2^{3+}\text{Si}_3\text{O}_{12}$ ) used by Höfer (2002) and Höfer and Brey (2007) are synthetic garnet end-members containing  $\text{Fe}^{3+}$  and  $\text{Fe}^{2+}$ , respectively. As shown by Höfer and Brey (2007), the flank positions determined by this “mineral-difference method” are consistent with self-absorption spectra calculated from X-ray emission spectra at different accelerating voltages. The ratio of intensities measured at the  $\text{FeL}\beta$  and  $\text{FeL}\alpha$  flank positions, expressed in this paper as  $L\beta/L\alpha$ , is a function of  $\text{Fe}^{2+}$  content. After some earlier attempts to correlate  $L\beta/L\alpha$  with  $\text{Fe}^{3+}/\Sigma\text{Fe}$  or  $\text{Fe}^{3+}$  content with the flank method (Höfer et al. 1994; Enders et al. 2000; Höfer 2002), the unambiguous and accurate quantification of  $\text{Fe}^{3+}/\Sigma\text{Fe}$  in garnet was demonstrated by Höfer and Brey

(2007). They also found that for different mineral groups (e.g., garnet, olivine, spinel, wüstite, etc.), the slopes of the regression lines of  $L\beta/L\alpha$  vs.  $\text{Fe}^{2+}$  content may differ significantly, implying that the correlation between  $L\beta/L\alpha$  and  $\text{Fe}^{2+}$  content might be a function of coordination number of  $\text{Fe}^{2+}$ . Therefore, to achieve the high precision and accuracy of measured Fe oxidation state as it is now achieved in garnets (Höfer and Brey 2007), it is necessary to calibrate the flank method for each mineral group and glass, i.e., for each crystal or non-crystal structure. While  $\text{Fe}^{2+}$  in garnet is eightfold coordinated, the coordination number of  $\text{Fe}^{2+}$  in silicate glasses is variable (4, 5, or 6, see Wilke et al. 2007). This difference in coordination between garnet and silicate glass needs to be examined before using garnets as standard materials for determining the Fe oxidation state of silicate glasses. As indicated by our tests (see below), the two garnet references (almandine and andradite) and several silicate glasses show a consistent correlation between  $L\beta/L\alpha$  and  $\text{Fe}^{2+}$  content. Therefore, we propose that garnets can be used as standards for measuring the Fe oxidation state of silicate glasses using the EPMA flank method.

## METHODS

### Sample selection

Two end-member garnets (Höfer and Brey 2007) with ferric (andradite,  $\text{Ca}_3^{2+}\text{Fe}_2^{3+}\text{Si}_3\text{O}_{12}$ ) and ferrous (almandine,  $\text{Fe}_3^{2+}\text{Al}_2^{3+}\text{Si}_3\text{O}_{12}$ ) iron were used to calibrate the flank method in this study. Forty-five silicate glasses belonging to five different glass groups were measured (Supplemental Table 1), including 29 Na- and K-free synthetic glasses (Borisov et al. 2004, 2015; Borisov 2007), 7 synthetic alkali-bearing glasses (ferrobasalts and basaltic andesite), 2 synthetic hydrous glasses, 4 re-melted natural glasses (MORB and basaltic), and 3 natural basaltic glass references from the Smithsonian Microbeam Standards collection (USNM 111240/52 VG-2, USNM 113498/1 VG-A99, and USNM 113716, Jarosewich et al. 1980). The synthesized or re-melted glasses were treated experimentally under controlled oxygen fugacity (see Supplemental Table 1 for experimental conditions and references), and these glasses cover a wide range of  $\text{FeO}_T$  content (4–18 wt%) and  $\text{Fe}^{2+}/\Sigma\text{Fe}$  ratio (0.2–1.0).

### Wet-chemistry analysis of Fe oxidation state

The oxidation state of Fe in all selected experimental glasses has been analyzed using a wet chemistry technique based on the colorimetric method of Wilson (1960) that was modified following the procedure given by Schuessler et al. (2008). The sample powders were first placed in an ammonium vanadate solution, which was then mixed with sulfuric acid. With additional HF, the mixed solution was sealed and kept overnight at room temperature. In this technique,  $\text{Fe}^{2+}$  is oxidized to  $\text{Fe}^{3+}$  due to the simultaneous reduction of  $\text{V}^{5+}$  to  $\text{V}^{4+}$ . Afterward, the excess HF in the solution was neutralized by adding saturated boric acid solution. The resultant solution was then mixed with quantified ammonium acetate solution, 2:2' bipyridyl solution and distilled water. The pH value in the solution was adjusted to  $\sim 5$  as buffered by ammonium acetate. The complex of  $\text{Fe}^{2+}$  with 2:2' bipyridyl shows an intensive absorption band at  $\sim 523$  nm, which allows quantification of  $\text{Fe}^{2+}$  by UV spectrometer. We used a Shimadzu UV-1800 spectrometer on the same solution to measure  $\text{Fe}^{2+}$  and total Fe before and after adding hydroxylamine hydrochloride solution (this reducing agent forces total Fe as  $\text{Fe}^{2+}$ ). This method ensures that the uncertainty in measured  $\text{Fe}^{2+}/\Sigma\text{Fe}$  is exclusively sourced from the spectrometric measurement but not related to weighing and dilution errors. An in-house standard andesite PU-3 (with known  $\text{Fe}^{2+}/\Sigma\text{Fe} = 0.39 \pm 0.03$ ; Schuessler et al. 2008) and USGS basaltic standard BHVO-1 ( $\text{Fe}^{2+}/\Sigma\text{Fe} = 0.77 \pm 0.03$ ) were measured over all analytical sessions, and the results were identical within the error.

### Electron probe microanalysis

Measurements of Fe oxidation state in silicate glasses using the flank method as well as the major element analyses have been performed with a Cameca SX100 electron microprobe equipped with five spectrometers and “PeakSight” operation software at the Institute of Mineralogy, Leibniz Universität Hannover, Germany. All standards and samples were coated with a thin carbon layer with a thickness of ca. 200 Å. The major elements (including total Fe as  $\text{FeO}_T$ ) were measured

using calibration standards of synthetic oxides ( $\text{Al}_2\text{O}_3$ ,  $\text{Fe}_2\text{O}_3$ ,  $\text{Mn}_3\text{O}_4$ ,  $\text{MgO}$ , and  $\text{TiO}_2$ ), natural wollastonite (for Si and Ca), orthoclase (for K), jadeite (for Na), and fluorapatite (for P). The quantifications of all major elements were based on  $K\alpha$  intensities, and raw data were corrected using the standard PAP procedure (Pouchou and Pichoir 1991). The accelerating voltage was set at 15 kV for measuring both the major elements and  $L\beta/L\alpha$ , as recommended by Höfer and Brey (2007). For alkali-free glasses, major elements were measured with a focused 15 nA beam (Borisov et al. 2004, 2015; Borisov 2007). For alkali-bearing glasses, we used a defocused beam (10  $\mu\text{m}$  diameter) and a lower current (10 nA) to minimize the loss of alkalis during electron bombardment of the sample surface. At least 10 points were measured on fresh surface of each sample (i.e., locations where not previously bombarded) to obtain averages and standard deviations for elemental analyses.

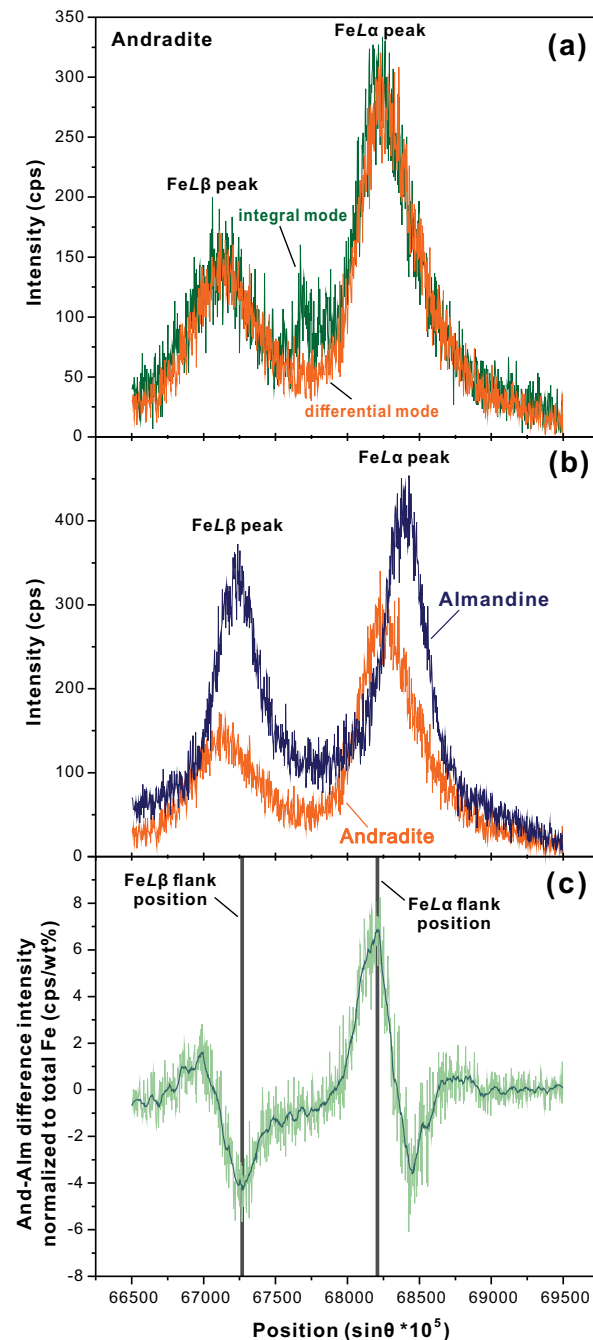
For flank method measurements, we first collected  $\text{Fe}L\alpha$  and  $\text{Fe}L\beta$  spectra in garnets. The settings of the TAP spectrometer were optimized to measure the  $\text{Fe}L$  lines according to the recipe given by Höfer and Brey (2007). This includes the optimization of the pulse-height analysis (PHA) setting for the  $\text{Fe}L\alpha$  line and the use of the “differential mode” for the X-ray counter. The differential mode was used to diminish high-energy X-ray lines (such as the ninth order of  $\text{Fe}K\alpha$  X-ray emission line) that are common when using the integral mode (Fig. 1a). A beam current of 200 nA and 10  $\mu\text{m}$  diameter was used to increase the intensity of the signal, and the sample stage was moved during analysis to diminish beam damage (see below).

As the *first step* of the method, the optimal positions of  $\text{Fe}L\alpha$  and  $\text{Fe}L\beta$  flanks were determined by collecting  $\text{Fe}L$  X-ray emission spectra of andradite and almandine. Figure 1b shows the results indicating that the relative positions and intensities of the  $\text{Fe}L\alpha$  and  $\text{Fe}L\beta$  peaks are displaced for both  $\text{Fe}^{2+}$  and  $\text{Fe}^{3+}$  end-members. Before subtracting the spectra to obtain the difference spectrum as described in Höfer and Brey (2007), we normalized the spectra to equal total Fe concentration (i.e., spectra intensity divided by mineral total Fe content) to compensate for the difference in bulk Fe contents between andradite and almandine. The resulting difference spectrum demonstrates minima and maxima (Fig. 1c). The most prominent minimum and maximum have been selected for the  $\text{Fe}L\beta$  and  $\text{Fe}L\alpha$  flank positions, respectively (vertical lines in Fig. 1c). The above difference spectra calculation has been measured with a relatively short acquisition time (1000 points, 5 accumulations, 100 ms dwell time). Therefore, the data points of the difference spectrum are scattered resulting in poorly defined flank positions.

In a *second step*, for achieving a better accuracy in defining the flank positions, we performed a flank position adjustment by measuring intensities along a shorter spectral range (from  $-60$  to  $+60$   $10^2 \times \sin\theta$  relative to the approximate flank positions determined in the first step) with a longer acquisition time (120 s). Figure 2 demonstrates that this procedure allows one to specify a peak position based on a more smoothed spectral pattern compared to the raw spectral scan data. In addition, this second-step adjustment shows that the new re-constrained minimum/maximum positions can be different from the approximate flank positions determined in the first step. As demonstrated by the tests on garnets of Höfer et al. (2000), slight changes in spectrometer position for measuring positions at the flanks would introduce significant variations in measured ratio  $L\beta/L\alpha$  between sessions. Due to various potential factors (such as drift of machine conditions, major changes in laboratory conditions, see Höfer and Brey 2007), the optimal flank positions vary between different analytical sessions, and therefore such flank position adjustment must be performed for each session independently. In addition, to avoid potential problems with oxidation-reduction induced by electron beam bombardment,

standards (garnets and glasses) need to be re-polished and carbon-coated before each session (see below).

We acquired the spectral intensities of  $\text{Fe}L\alpha$  and  $\text{Fe}L\beta$  at the re-constrained flank positions for both garnet standards and unknown silicate glasses using a beam current of 200 nA and a counting time of 120 s. This high beam current immediately poses the question whether beam damage is significant. Beam damage is well known to be a problem for analyzing alkali-bearing glasses (Morgan and London 1996). For example, in several publications, Fialin and co-authors thoroughly discussed the role of beam-induced Fe oxidation or/and reduction caused by electromigration of alkalis during EPMA analysis (Fialin et al. 2004, 2001; Fialin and Wagner 2012). Surprisingly, the same authors reported, “neither oxidation-induced nor reduction-induced peak shifts” during measurements of dry and hydrous glasses utilized for the calibration of their peak shift method (Fialin et al. 2011; operating conditions were: 15 kV accelerating potential, 250 nA beam current, 20  $\mu\text{m}$  beam diameter,



► **FIGURE 1.**  $\text{Fe}L$  X-ray emission spectra of andradite ( $\text{Ca}_3^{2+}\text{Fe}_3^{3+}\text{Si}_3\text{O}_{12}$ ) and almandine ( $\text{Fe}_3^{3+}\text{Al}_2^{3+}\text{Si}_3\text{O}_{12}$ ) acquired at 15 kV, beam current 200 nA, and beam size 10  $\mu\text{m}$ . (a) Comparison of PHA integral mode and differential mode for  $\text{Fe}L$  X-ray emission spectra of andradite. Note that, for integral mode, there is a small peak between the major  $\text{Fe}L\alpha$  and  $\text{Fe}L\beta$  peaks, which is the ninth order of the high-energy  $\text{Fe}K\alpha$  X-ray emission line. (b) Spectra of andradite and almandine acquired in a differential mode so the high-energy  $\text{Fe}K\alpha$  X-ray emission line was diminished. Baseline = 1100 mV, window = 1300 mV, beam current 200 nA, beam size 10  $\mu\text{m}$ , dwell time 0.1 s, accumulation number 5. (c) Difference spectrum (original spectra were acquired with differential mode) between andradite and almandine normalized to equal total Fe content (light in color). Smoothed spectrum (dark in color) is obtained by the Savitzky-Golay method (Savitzky and Golay 1964). The flank positions of  $\text{Fe}L\alpha$  and  $\text{Fe}L\beta$  are found at the maximum and minimum of the smoothed difference spectrum (marked by the vertical lines).

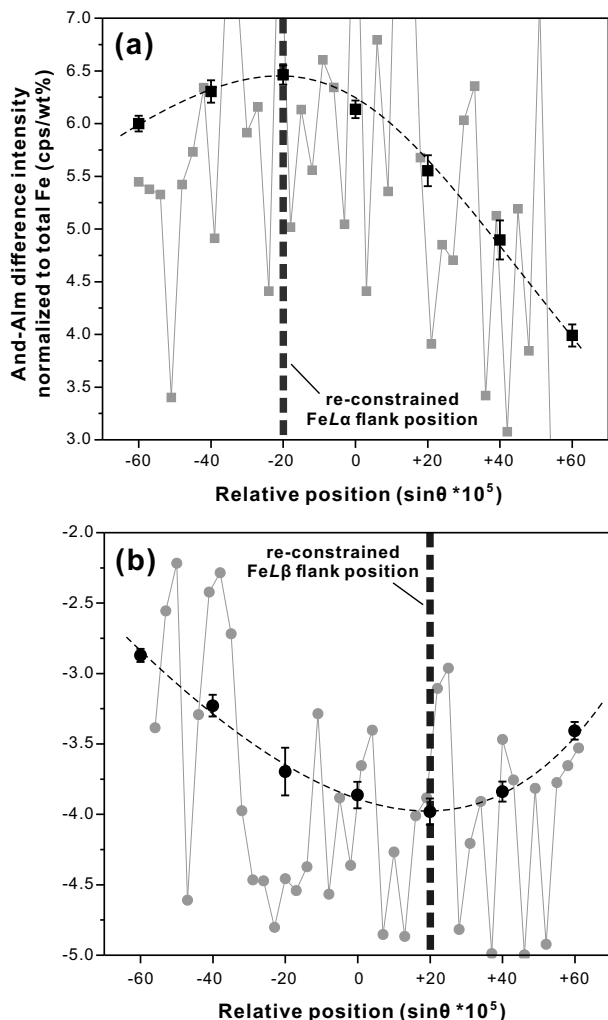


**FIGURE 2.** Re-constrained flank positions of FeLa (a) and FeLβ (b) based on andradite and almandine. The initial flank positions (relative position = 0) are determined by smoothed difference spectra (see Fig. 1c). At positions of 0, ±20, ±40, and ±60 relative to the initial flank positions, andradite and almandine were analyzed again with a longer counting time (120 s each, three repeated measurements) to obtain more accurate difference spectra (spots with ±1σ deviation and dashed curve). For comparison, the short-time scan spectra are shown in light gray. See text for details.

and counting time 240 s). Using static sample stage (conventional analysis, when the same analytical spot is exposed to the beam for the whole acquisition time), we applied the Fialin et al.'s (2011) protocol of peak-shift method to our set of experimental glasses, however we failed to observe a robust correlation between the shift of FeLa peak position and Fe oxidation state, which suggests that the calibration of Fialin et al. (2011) should be revised on a more extensive data set (see Supplemental<sup>1</sup> Fig. 1). Thus, our first test measurements clearly demonstrated that beam-induced oxidation/reduction needs to be seriously considered. In this study, to minimize the beam damage, we suggest moving the sample stage with a rate of 2 μm/s during acquisition (see also discussion below). Three independent measurements on different areas (~240×10 μm<sup>2</sup>) have been performed for each sample. To check the reproducibility between sessions, analyses of a few samples were replicated during three different analytical sessions (Supplemental<sup>1</sup> Table 2) with a time gap of approximately one month. The ratio of intensities, Lβ/Lα, measured at the FeLβ and FeLa flank positions was then calculated and used for quantifying the Fe oxidation state.

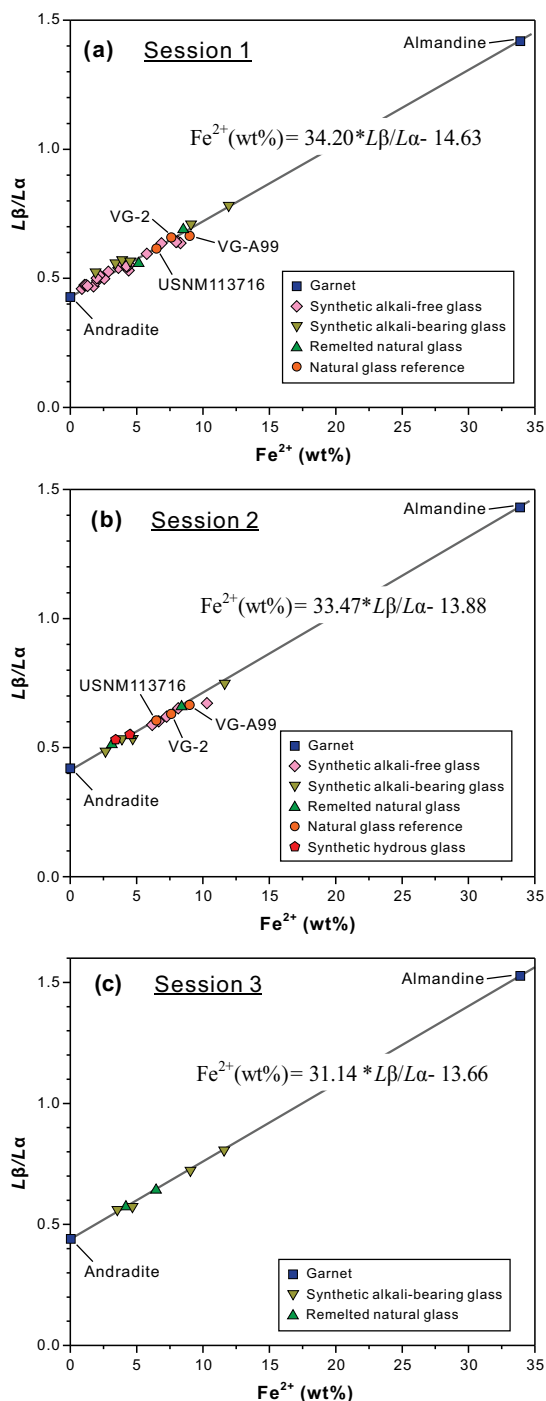


**FIGURE 3.** Plots of Lβ/Lα vs. Fe<sup>2+</sup> content for garnets and glasses. Data measured in Session 1 (a), Session 2 (b), and Session 3 (c). Deviation of ±1σ is smaller than symbol size. See details in Supplemental<sup>1</sup> Table 1.

## RESULTS

To test the flank method described above, we have measured Lβ/Lα of the garnet standards and the five silicate glass groups with known Fe oxidation state (Supplemental<sup>1</sup> Table 2). As shown in Figure 3, the values of Lβ/Lα and Fe<sup>2+</sup> content vary linearly in all

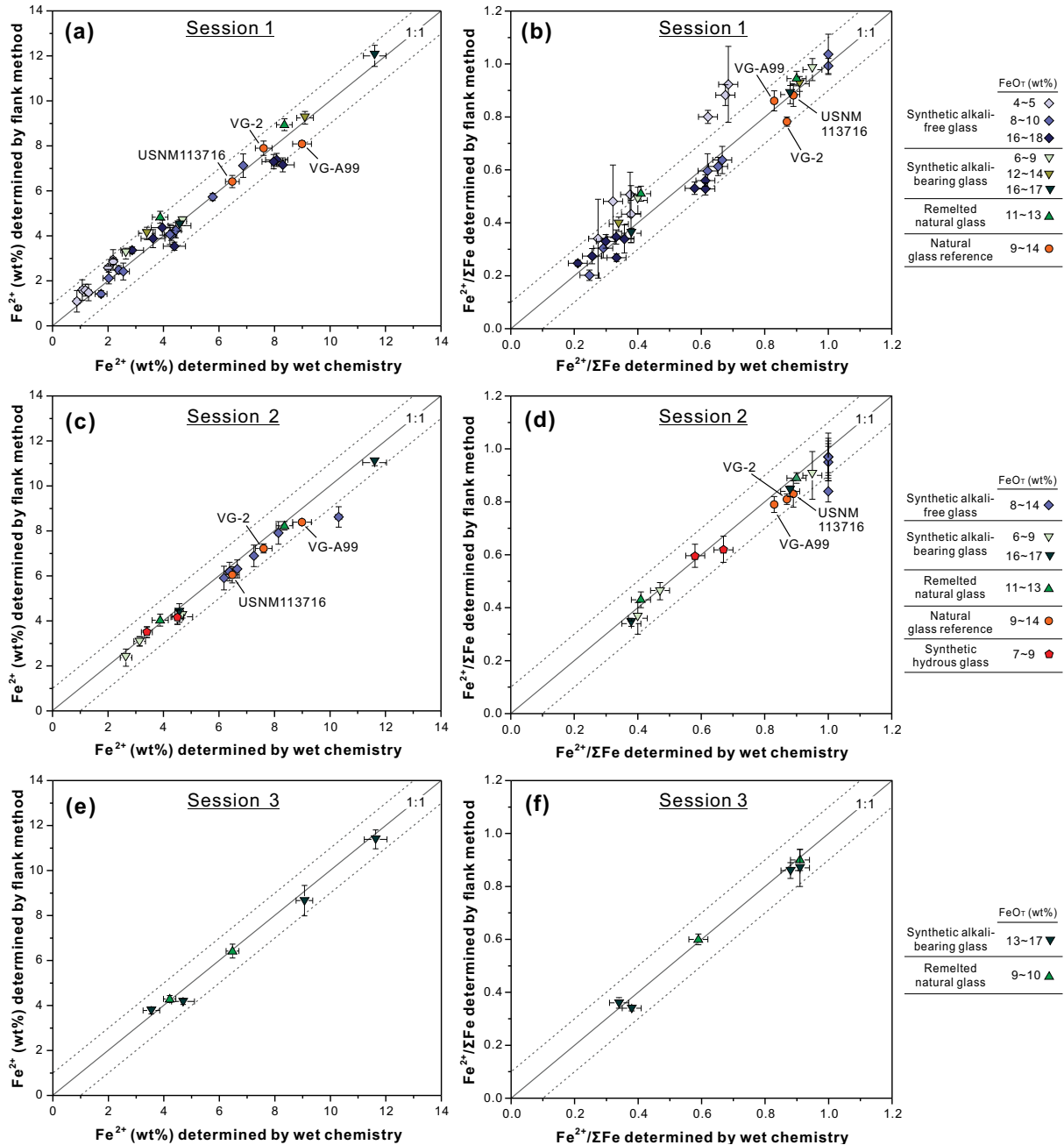


**FIGURE 4.** Comparison of glass  $\text{Fe}^{2+}$  content and  $\text{Fe}^{2+}/\Sigma\text{Fe}$  ratio determined by EPMA flank method and wet chemistry. Data measured in Session 1 (a and b), Session 2 (c and d), and Session 3 (e and f). The dashed line is  $\pm 1$  wt% in the left panels and  $\pm 0.1$  in the right panels.

sessions. Moreover, all measured glasses lie closely on the trends defined by the garnet standards, indicating that well-characterized garnet end-members can be used as calibrating standards to quantify the Fe oxidation state in silicate glasses despite their different coordination of iron cation. The linear relations defined by the garnet standards for the three independent sessions are:

$$\text{Fe}^{2+} (\text{wt}\%) = 34.20 \times L\beta/L\alpha - 14.63 \quad (\text{Session 1})$$

$$\text{Fe}^{2+} (\text{wt}\%) = 33.47 \times L\beta/L\alpha - 13.88 \quad (\text{Session 2})$$

$$\text{Fe}^{2+} (\text{wt}\%) = 31.14 \times L\beta/L\alpha - 13.66 \quad (\text{Session 3}).$$

Using these relations and  $\text{FeO}_T$  concentrations in the glasses, the  $\text{Fe}^{2+}$  contents and corresponding  $\text{Fe}^{2+}/\Sigma\text{Fe}$  ratios can be calculated (Supplemental Table 2). Figures 4a, 4c, and 4e show that the  $\text{Fe}^{2+}$  contents determined by the flank method are consistent within error with those determined by wet chemistry in most cases, and the differences are in general less than 1 wt% for all silicate glasses. Figures 4b, 4d, and 4f show that the  $\text{Fe}^{2+}/\Sigma\text{Fe}$  ratios determined by the flank method are consistent within a value of  $\pm 0.1$  with those determined by wet chemistry for samples with high  $\text{FeO}_T$  contents ( $> 5$  wt%), whereas the ratio difference

increase to 0.2–0.3 for samples with lower  $\text{FeO}_T$  contents. This implies that the error of the  $\text{Fe}^{2+}/\Sigma\text{Fe}$  determined by the flank method is dominantly associated with the intensity measured at the  $\text{Fe}L$  flanks; i.e., the lower the  $\text{FeO}_T$  content, the lower the accuracy of the analysis.

## DISCUSSION

Potential errors of determining  $\text{Fe}^{2+}/\Sigma\text{Fe}$  ratio of glasses using the EPMA flank method can be related to compositional effects that denote self-absorption of  $\text{Fe}L$  lines by Fe and variable absorption of  $\text{Fe}L$  lines by other cations (Höfer et al. 1994; Fialin et al. 2001). To investigate potential compositional effects, we plotted the difference between  $\text{Fe}^{2+}$  measured by EPMA and wet chemistry ( $\Delta\text{Fe}^{2+}$ ) against total Fe content in Figure 5. The data do not show any apparent correlation between the measured  $\text{Fe}^{2+}$  and  $\text{FeO}_T$  contents, therefore no systematic discrepancy between glasses with contrasting  $\text{FeO}_T$  contents. This implies that our method of  $\text{Fe}^{2+}$  determination with the above linear equations is robust and total Fe has little effect on this calibration. As shown by Höfer and Brey (2007),  $L\beta/L\alpha$  does depend on total Fe, but this effect can be split into the dependence on  $\text{Fe}^{2+}$  and  $\text{Fe}^{3+}$  (due to different self-absorption) and can be approximated by a simple linear equation at low total Fe cases (e.g.,  $\text{FeO}_T < 20$  wt%).

We explored the potential effect of Ti on the flank method on differentially absorbing  $\text{Fe}La$  and  $\text{Fe}L\beta$  within silicate glasses, we explored it within the range of  $\text{TiO}_2$  content between 0 and 25 wt%. As listed in Supplemental<sup>1</sup> Table 2, for silicate glasses with  $\text{TiO}_2$  contents lower than 15 wt%, no systematic correlation is observed between  $\Delta\text{Fe}^{2+}$  and  $\text{TiO}_2$  content. However, sample DAT32 with extremely high  $\text{TiO}_2$  (25.09 wt%) demonstrates high  $\Delta\text{Fe}^{2+}$  (Fig. 5b), suggesting that Ti is indeed able to influence the absorption of  $\text{Fe}La$  and/or  $\text{Fe}L\beta$ , but only for silicate glasses with very high  $\text{TiO}_2$  contents (at least >15 wt%). Although Fialin et al. (2001) emphasized the potential effect of Cr and Ti on Fe  $L$  line emission and absorption, this problem is perhaps only crucial for Cr- and/or Ti-rich phases (e.g., chromite and ilmenite). The absorption effect of Ti should be extremely weak in silicate glasses with low Ti contents, as demonstrated by the data of Fialin et al. (2004) involving silicate glasses with 0–1.8 wt%  $\text{TiO}_2$ . This assumption is supported by our results.

Potential matrix effects of other elements such as Si, Al, Ca, and Mg on the flank method for glasses were not observed in this study, which is consistent with the observations of Höfer and Brey (2007) on garnets. The data set of silicate glass in this study covers a relatively wide compositional range (Supplemental<sup>1</sup> Table 1), in terms of  $\text{SiO}_2$  (40–56 wt%),  $\text{Al}_2\text{O}_3$  (10–18 wt%), CaO (9–23 wt%), and MgO (4–10 wt%), and no systematic influence of these major oxides on  $L\beta/L\alpha$  in the range of  $\text{FeO}_T$  (4–18 wt%) was observed. To conclude, our measurements demonstrate that  $\text{Fe}^{2+}$  in silicate glasses can be calculated from  $L\beta/L\alpha$  based on the quantitative relation calibrated against  $\text{Fe}^{2+}$ -rich and  $\text{Fe}^{3+}$ -rich garnet end-members, and there is no significant matrix effect of other cations, except for Ti, if it is present in very high abundances.

Applying the peak-shift method, Fialin et al. (2004) observed both apparent oxidation and reduction trends with accumulated analytical time (at a 15 kV accelerating voltage, 240 nA beam current and 20  $\mu\text{m}$  beam diameter). The observed variation of measured Fe oxidation state with time was attributed by Fialin

et al. (2004) to two factors, including (1) Na migration and consequent rearrangement of oxygen atoms between bridging and non-bridging positions in the close vicinity of electron beam bombardment, and (2) buildup of carbon contamination. In this study, we performed additional tests on the anhydrous natural glass reference VG-2 (0.02 wt%  $\text{H}_2\text{O}$ ; Fig. 6) and on basaltic glasses with 0, 2.8 and 5.0 wt%  $\text{H}_2\text{O}$  (Fig. 7) to illustrate the potential beam damage at 200 nA beam current and associated effects on measurements of  $L\beta/L\alpha$ , in two contrasting cases with a static sample stage (points in Figs. 6 and 7) and with a moving stage (horizontal dashed line in Figs. 6 and 7).

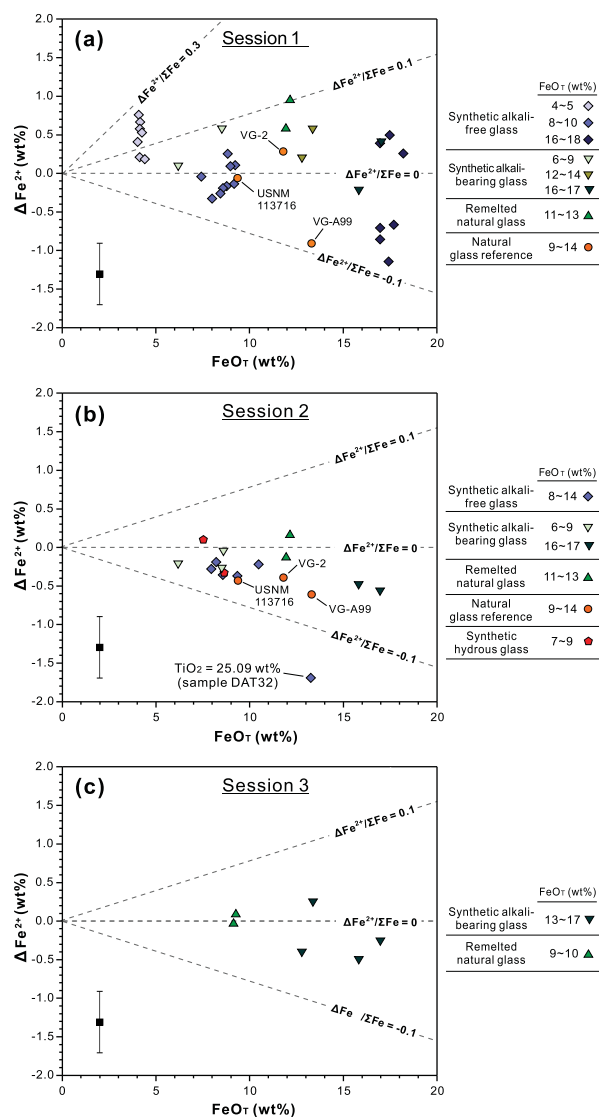


**FIGURE 5.** The difference of  $\text{Fe}^{2+}$  content (i.e.,  $\Delta\text{Fe}^{2+}$ ) between EPMA flank method and wet chemistry plotted against  $\text{FeO}_T$  content (see data in Supplemental<sup>1</sup> Table 1). Data measured in Session 1 (a), Session 2 (b), and Session 3 (c) are plotted separately. Isoleths of induced  $\Delta\text{Fe}^{2+}/\Sigma\text{Fe}$  are also noted in the left panels. The mean standard deviation of calculated  $\Delta\text{Fe}^{2+}$  is  $\sim 0.4$  (see inserted error bar). The standard deviation of  $\text{FeO}_T$  content is smaller than symbol size.

As shown in the left-side panels of Figure 6, the values of  $L\beta/L\alpha$  measured with a beam diameter from 5 to 20  $\mu\text{m}$  show different behavior with time for the anhydrous basaltic glass VG-2, with the sample stage being static for each measurement. The 5  $\mu\text{m}$  beam induces an overall decrease of  $L\beta/L\alpha$  after 250 s, which likely indicates oxidation of the analytical volume due to electron beam bombardment. In contrast, the use of a 10 or 20  $\mu\text{m}$  beam tends to increase slightly (or does not modify) the measured ratio of  $L\beta/L\alpha$  during the first 250 s. The right-side panels in Figure 6 show variations of the intensities of  $\text{Fe}K\alpha$  and  $\text{Na}K\alpha$  for the beam diameters of 5, 10, and 20  $\mu\text{m}$ , which can provide information on interpreting the variations of  $L\beta/L\alpha$ . One striking observation is that the loss of the  $\text{Na}K\alpha$  intensity occurs for all beam sizes, and it is enhanced with decreasing beam size, consistent with previous studies (e.g., Morgan and London 1996; Fialin et al. 2004). In addition, we show that the  $\text{Fe}K\alpha$  intensity slightly increases when the 5 and 10  $\mu\text{m}$  beams were used, and it remains almost constant with the 20  $\mu\text{m}$  beam, demonstrating the tendency of increasing relative Fe content in glass with increase of beam current (probably due to alkali loss and changes of glass density), similar to what has been also shown for  $\text{Si}K\alpha$  and  $\text{Al}K\alpha$  (Morgan and London 1996; Zhang et al. 2016). Provided that  $L\beta/L\alpha$  is positively correlated with  $\text{Fe}^{2+}$  content, it seems that severe beam damage (both Na

intensity loss and Fe intensity increase) with a small beam size (i.e., 5  $\mu\text{m}$ ) tends to oxidize the analyzed glass volume (decreasing  $\text{Fe}^{2+}/\Sigma\text{Fe}$  ratio), whereas weak beam damage (only slight Na intensity loss and no Fe intensity increase) with a large beam size (i.e., 20  $\mu\text{m}$ ) tends to reduce (or not modify) the analyzed glass volume (increasing  $\text{Fe}^{2+}/\Sigma\text{Fe}$  ratio).

It is well known that the migration of Na during EPMA (i.e., loss of Na intensity) is much stronger in hydrous glasses than in dry glasses, even if the beam current is as low as 2–5 nA (Morgan and London 1996). On the other hand, water as a chemical component has almost negligible effect on the ferric/ferrous ratio of silicate glasses (Botcharnikov et al. 2005). In this study, we conducted a test of beam damage as a function of time on three glasses with similar major element compositions but different  $\text{H}_2\text{O}$  contents (nominally dry, 2.8 and 5.0 wt%  $\text{H}_2\text{O}$ , Supplemental<sup>1</sup> Table 1). The  $L\beta/L\alpha$  values and  $\text{Fe}K\alpha$  and  $\text{Na}K\alpha$  intensities have been acquired at 200 nA and 20  $\mu\text{m}$  beam diameter over 500 s with the sample stage being static, which are compared to the values obtained while moving the sample stage. The left-side panels of Figure 7 show the variation of  $L\beta/L\alpha$ , and the right-side panels show the variation of intensities of  $\text{Fe}K\alpha$  and  $\text{Na}K\alpha$ . With an increase of  $\text{H}_2\text{O}$  content, the loss of Na intensity is dramatically enhanced and  $\text{Fe}K\alpha$  intensity tends to increase. The value of  $L\beta/L\alpha$  increases slightly during the

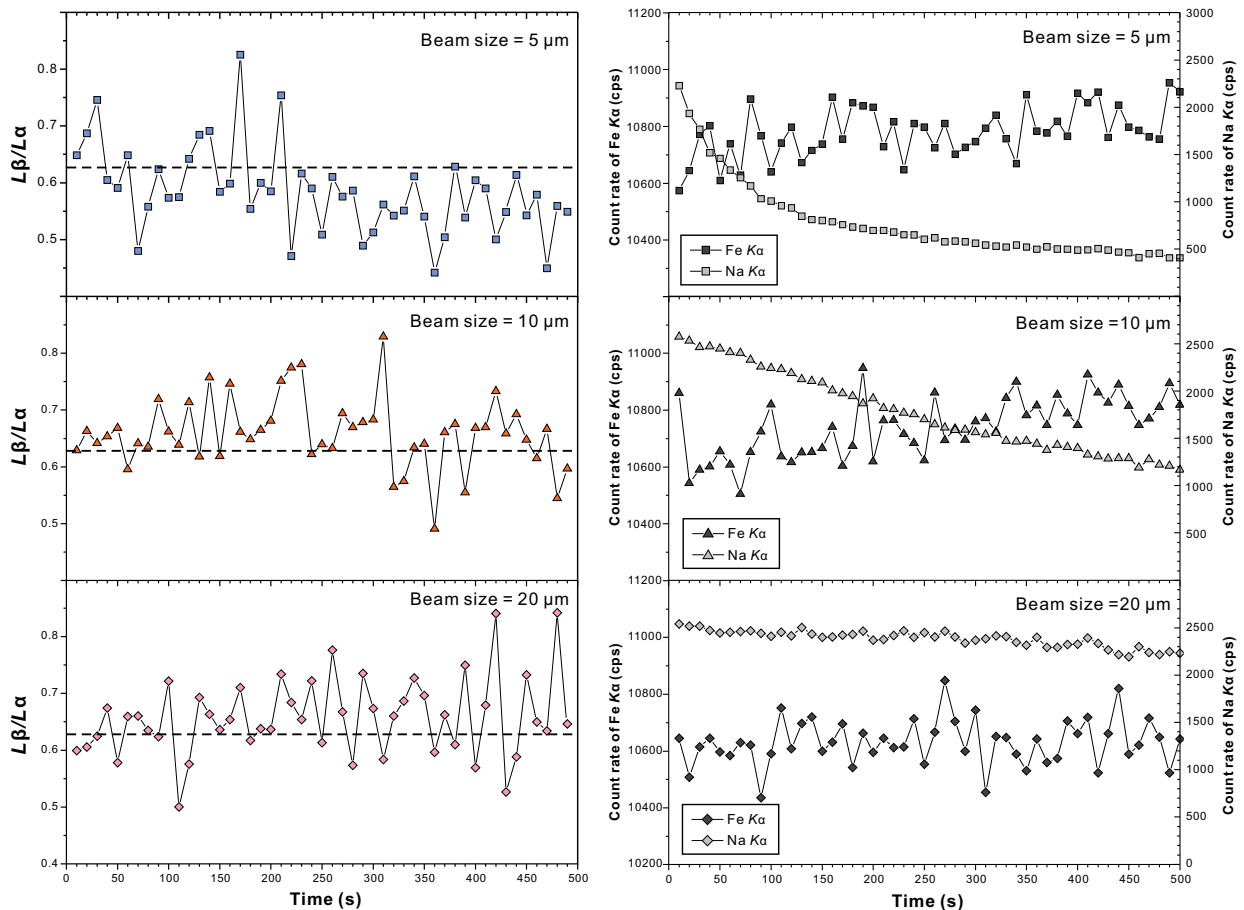


**FIGURE 6.** Variation of  $L\beta/L\alpha$  and count rates of  $\text{Fe}K\alpha$  and  $\text{Na}K\alpha$  as a function of time measured with different beam size for reference glass VG-2. Beam setting is 15 kV and 200 nA for all cases. Dashed line indicates the mean value of  $L\beta/L\alpha$  measured with moving sample stage, in which case beam damage is minimized.

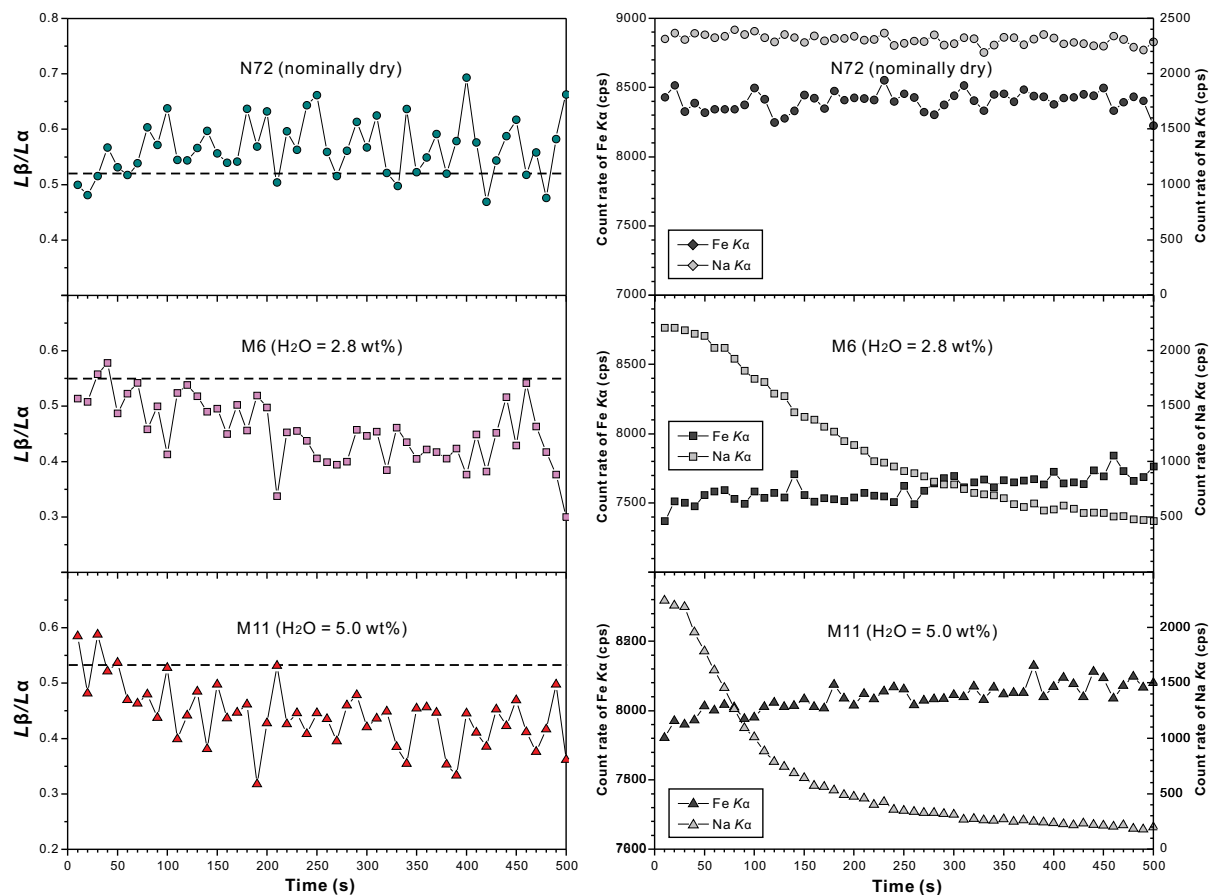


**FIGURE 7.** Variation of  $L\beta/L\alpha$  and count rates of  $FeK\alpha$  and  $NaK\alpha$  as a function of time measured for three glasses (M72, M6, and M11, Shishkina et al. 2010) with different  $H_2O$  contents but similar major element composition. Beam current is 200 nA and beam size is 20  $\mu m$  diameter for all cases. Dashed lines indicate the mean value of  $L\beta/L\alpha$  measured with moving sample stage, in which case beam damage is minimized.

first 100 s on nominally dry glass N72, consistent with the results obtained on the VG-2 sample measured with a 20  $\mu m$  diameter beam (Fig. 6). In contrast, in  $H_2O$ -bearing glasses the  $L\beta/L\alpha$  value decreases significantly within the same time period, indicating a decrease of  $Fe^{2+}$  content in spite of increasing relative total Fe content in the glass as inferred from increasing  $FeK\alpha$  intensity. As shown in Figure 8, the strong decreases in  $NaK\alpha$  intensity and  $L\beta/L\alpha$  are roughly coupled for the hydrous glasses, supporting the hypothesis that the migration of Na during EPMA might promote oxidation of  $Fe^{2+}$  converted to  $Fe^{3+}$  (Fialin et al. 2004). Therefore, in comparison to dry glasses, the analyzed volume of hydrous glass is much more prone to be oxidized during EPMA as a result of beam damage.

Besides the potential effect of Na-migration on the EPMA measurement of Fe  $L\beta/L\alpha$  ratio of silicate glasses discussed above, carbon contamination or loss on C-coated sample surface could also play a significant role. Gopon et al. (2013) showed that carbon contamination is a serious problem affecting the measured stabilities of  $FeL\alpha$  and  $FeL\beta$  of Fe-Si compounds, especially in cases where a static high-current beam is used. Fialin et al. (2004) found a buildup of carbon contamination on silicate glass to be significant when measurements were performed with a 240 nA beam current (20  $\mu m$  diameter) on the same spot. They

suggested that it might have partly resulted in the decrease of measured  $Fe^{3+}/\Sigma Fe$  ratio using their peak-shift method, at least for the initial stage of measurement time. Höfer and Brey (2007) made a similar test on an almandine sample with a 60 nA beam scanning an area of  $3 \times 5 \mu m^2$ , and they demonstrated that carbon contamination resulted in a decrease in  $L\beta/L\alpha$  ratio measured by their flank method and in overestimation of  $Fe^{3+}/\Sigma Fe$  ratio. Interestingly, the effect of carbon contamination on measuring the Fe oxidation state, observed by Fialin et al. (2004) for silicate glass and by Höfer and Brey (2007) for garnet are contradicting with each other. We tested carbon contamination by measuring the  $CK\alpha$  intensity on the VG-2 glass with static and moving sample stage, respectively. As shown in Figure 9, the  $CK\alpha$  intensity measured on the same spot (i.e., with static sample stage) decreases strongly and continuously with accumulated time up to 400 s, whereas the measurements with moving sample stage demonstrate constant intensity. The observed decrease of  $CK\alpha$  intensity during beam bombardment is contradicting with Fialin et al. (2004) but consistent with that observed by Gopon et al. (2013). Fialin et al. (2004) observed a continuous increase of  $CK\alpha$  intensity on a silicate glass for 15 min. However, Gopon et al. (2013) made tests on carbon-coated FeSi compounds with a low-voltage high-current beam (5 kV, 100 nA) and found  $CK\alpha$

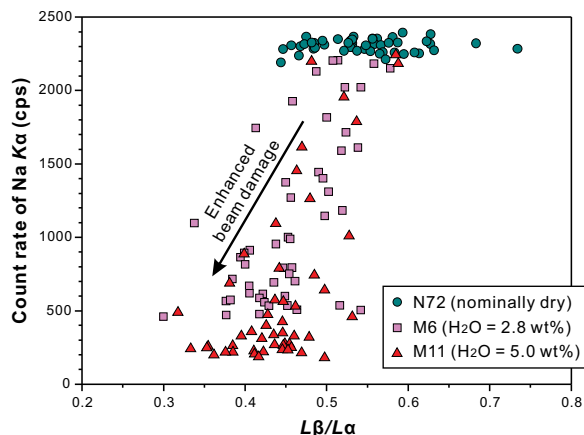


**FIGURE 8.** Plots of  $L\beta/L\alpha$  vs. count rate of NaK $\alpha$  for glasses M72, M6, and M11. Beam current is 200 nA and beam size is 20  $\mu\text{m}$  diameter for all cases. The values are for various times during time series measurements, with highest Na signal at the beginning and lowest Na signal at the ending point.

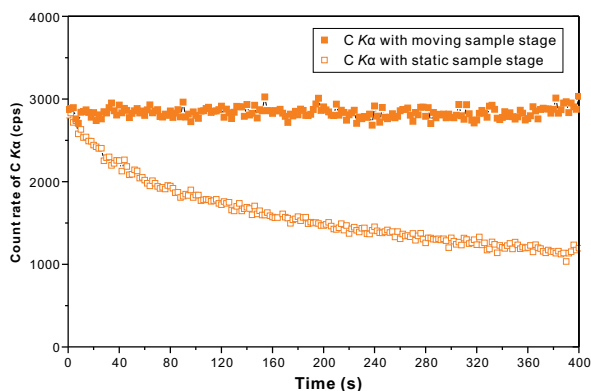


**FIGURE 9.** Count rate variations of CK $\alpha$  as a function of time measured acquired on VG-2 glass. Beam current and diameter are 200 nA and 20  $\mu\text{m}$ , respectively. Note the contrasting variation trends obtained with moving and static sample stage, respectively.

intensity was first strongly lost in the initial 400 s but gained later on with accumulated time up to 4000 s. Therefore, the effect of carbon contamination or loss seems to be complicated and probably depends on several factors, such as material composition, beam current, time, etc. In any case, for applying the flank method described in this paper, carbon contamination and loss should be avoided to measure glass Fe  $L\beta/L\alpha$  ratios, and moving the sample stage is demonstrated to be a good approach.

Based on these results, we conclude that, if the EPMA measurements are carried out at the same position for a long time on glasses, the variation of  $L\beta/L\alpha$  is a consequence of the combined effects of the changes in both total Fe content and Fe oxidation state of glass, reflecting accumulated material damage induced by electron beam bombardment. Our tests conducted with a static stage demonstrate that the values of  $L\beta/L\alpha$  cannot be accurately resolved for dry or hydrous glasses if a high beam current and a long acquisition time are applied. However, our results show that a high accuracy in the determination of the  $L\beta/L\alpha$  (and thus

**TABLE 1.** Possible errors in  $f_{\text{O}_2}$  determination using the flank method for MORB glasses

$\text{Fe}^{2+}/\Sigma\text{Fe}$	$\text{FeO}_T = 10 \text{ wt}\%$		$\text{FeO}_T = 9 \text{ wt}\%$		$\text{FeO}_T = 8 \text{ wt}\%$	
	$\Delta\text{Fe}^{2+}/\Sigma\text{Fe}^a$	$\Delta\log f_{\text{O}_2}^b$	$\Delta\text{Fe}^{2+}/\Sigma\text{Fe}$	$\Delta\log f_{\text{O}_2}$	$\Delta\text{Fe}^{2+}/\Sigma\text{Fe}$	$\Delta\log f_{\text{O}_2}$
0.95	0.13	0.30	0.14	0.33	0.16	0.37
0.90	0.13	0.16	0.14	0.17	0.16	0.19
0.85	0.13	0.11	0.14	0.12	0.16	0.14
0.80	0.13	0.09	0.14	0.10	0.16	0.11
0.75	0.13	0.07	0.14	0.08	0.16	0.07

<sup>a</sup> Assumed  $\Delta\text{Fe}^{2+} = 1 \text{ wt}\%$  ( $2\sigma$ , flank method, EPMA) and  $\Delta\Sigma\text{Fe} = 1 \text{ wt}\%$  (EPMA).

<sup>b</sup> Assumed ideal slope of 0.25 for  $\log(\text{Fe}^{3+}/\text{Fe}^{2+})$  vs.  $\log f_{\text{O}_2}$ .

Fe $^{2+}/\Sigma\text{Fe}$  ratio) can be achieved when analyses are conducted with a continuously moving sample stage (e.g., 2  $\mu\text{m}/\text{s}$ ) during data acquisition.

## IMPLICATIONS

When the beam damage problem is successfully resolved (e.g., by movement of the sample stage in this study), the EPMA flank method provides a promising low-cost and very simple alternative to other local non-destructive techniques, such as XANES, micro-Mössbauer spectroscopy, EELS, and micro-Raman spectroscopy (see introduction for the references). In this study, the accuracy of the Fe $^{2+}/\Sigma\text{Fe}$  determination is found to be dependent both on the Fe $^{2+}$  content determined with the flank method and on the total Fe content, and is generally within  $\pm 0.1$  for silicate glasses with FeO $_T > 5 \text{ wt}\%$ .

In petrology, accurately determined Fe $^{2+}/\Sigma\text{Fe}$  ratio in natural glasses serves as a proxy of the redox conditions ( $f_{\text{O}_2}$ ) prevailing in magmatic chambers (Christie et al. 1986; Bézou and Humler 2005; Cottrell and Kelley 2011). For example, the most recent data obtained by Cottrell and Kelley (2011) by XANES for naturally quenched pillow-rim glasses suggest that global MORB Fe $^{2+}/\Sigma\text{Fe}$  has a value of  $0.84 \pm 0.01$  ( $1\sigma$ ) corresponding to the fayalite–magnetite–quartz (FMQ) buffer under conditions of primary magma generation. Assuming 1 wt% error ( $2\sigma$ ) in the determination of Fe $^{2+}$  by the flank EPMA method and an ideal slope of  $1/4$  for the dependence between  $\log(\text{Fe}^{3+}/\text{Fe}^{2+})$  and  $\log f_{\text{O}_2}$  we provide propagated errors in the determination of  $f_{\text{O}_2}$  for the range of Fe $^{2+}/\Sigma\text{Fe}$  values typical for natural melts (Table 1). Note, however, that additional errors may result from the application of empirical models describing the dependence of ferric/ferrous ratios on temperature, oxygen fugacity, and melt composition, and also from differences between real pre-eruptive temperatures of basaltic melts and the temperature of 1200 °C typically assumed for  $\Delta\text{FMQ}$  calculations (see discussion in Borisov et al. 2013). As one can see, the translated uncertainties in estimation of the oxygen fugacity for typical MORB (Fe $^{2+}/\Sigma\text{Fe} \sim 0.85$ ; FeO $_T \approx 9 \text{ wt}\%$ ) range within only  $\pm 0.12 \log$  units ( $2\sigma$ ). This high precision in the determination of the Fe $^{2+}/\Sigma\text{Fe}$  and, in turn,  $f_{\text{O}_2}$  by the flank EPMA method also provides a new promising analytical tool for future experimental studies under high pressures, where controlling and logging the redox conditions is usually a challenging task.

## ACKNOWLEDGMENTS

We thank Marius Stranghöner and Florian Pohl for the help with the wet-chemistry colorimetric method and Julian Feige for sample preparation. We appreciate editorial work of Maurizio Petrelli as well as detailed and insightful comments from John Fournelle and two anonymous reviewers. R.A. thanks Anette von der Handt and Eric Hellebrandt for support of the project. This study was funded by DFG projects AL1189/6-1, AL1189/8-1, AL1189/9-1, and HO1337/35-1.

## REFERENCES CITED

- Almeev, R.R., Holtz, F., Ariskin, A., and Kimura, J.-I. (2013) Storage conditions of Bezymianny Volcano parental magmas: results of phase equilibria experiments at 100 and 700 MPa. *Contributions to Mineralogy and Petrology*, 166(5), 1389–1414.
- Almeev, R.R., Holtz, F., Koepke, J., Parat, F., and Botcharnikov, R.E. (2007) The effect of H<sub>2</sub>O on olivine crystallization in MORB: Experimental calibration at 200 MPa. *American Mineralogist*, 92(4), 670–674.
- Bézos, A., and Humler, E. (2005) The Fe<sup>3+</sup>/ΣFe ratios of MORB glasses and their implications for mantle melting. *Geochimica et Cosmochimica Acta*, 69, 711–725.
- Borisov, A.A. (2007) Experimental study of the influence of SiO<sub>2</sub> on the solubility of cobalt and iron in silicate melts. *Petrology*, 15(6), 523–529.
- Borisov, A.A., and Shapkin, A.I. (1990) A new empirical equation rating Fe<sup>3+</sup>/Fe<sup>2+</sup> in magmas to their composition, oxygen fugacity and temperature. *Geochemistry International*, 27, 111–116.
- Borisov, A., Lahaye, Y., and Palme, H. (2004) The effect of TiO<sub>2</sub> on Pd, Ni, and Fe solubilities in silicate melts. *American Mineralogist*, 89(4), 564–571.
- Borisov, A., Behrens, H., and Holtz, F. (2013) The effect of titanium and phosphorus on ferric/ferrous ratio in silicate melts: an experimental study. *Contributions to Mineralogy and Petrology*, 166(6), 1577–1591.
- Borisov, A., Behrens, H., and Holtz, F. (2015) Effects of melt composition on Fe<sup>3+</sup>/Fe<sup>2+</sup> in silicate melts: a step to model ferric/ferrous ratio in multicomponent systems. *Contributions to Mineralogy and Petrology*, 169(2), 1–12.
- Botcharnikov, R.E., Koepke, J., Holtz, F., McCammon, C., and Wilke, M. (2005) The effect of water activity on the oxidation and structural state of Fe in a ferro-basaltic melt. *Geochimica et Cosmochimica Acta*, 69(21), 5071–5085.
- Botcharnikov, R.E., Almeev, R.R., Koepke, J., and Holtz, F. (2008) Phase relations and liquid lines of descent in hydrous ferrobasalt—implications for the Skaergaard Intrusion and Columbia River Flood Basalts. *Journal of Petrology*, 49(9), 1687–1727.
- Christie, D.M., Carmichael, I.S.E., and Langmuir, C.H. (1986) Oxidation states of mid-ocean ridge basalt glasses. *Earth and Planetary Science Letters*, 79, 397–411.
- Cottrell, E., and Kelley, K.A. (2011) The oxidation state of Fe in MORB glasses and the oxygen fugacity of the upper mantle. *Earth and Planetary Science Letters*, 305(3–4), 270–282.
- Di Muro, A., Métrich, N., Mercier, M., Giordano, D., Massare, D., and Montagnac, G. (2009) Micro-Raman determination of iron redox state in dry natural glasses: Application to peralkaline rhyolites and basalts. *Chemical Geology*, 259(1), 78–88.
- Ejima, T., Akasaka, M., and Ohfuiji, H. (2011) Oxidation state of Fe in olivine in a lherzolite xenolith from Oku district, Oki-Dogo Island, Shimane Prefecture, Japan. *Journal of Mineralogical and Petrological Sciences*, 106(5), 246–254.
- Enders, M., Speer, D., Maresch, W.V., and McCammon, C.A. (2000) Ferric/ferrous iron ratios in sodic amphiboles: Mössbauer analysis, stoichiometry-based model calculations and the high-resolution microanalytical flank method. *Contributions to Mineralogy and Petrology*, 140(2), 135–147.
- Fialin, M., and Wagner, C. (2012) Redox kinetics of iron in alkali silicate glasses exposed to ionizing beams: Examples with the electron microprobe. *Journal of Non-Crystalline Solids*, 358, 1617–1623.
- Fialin, M., Wagner, C., Métrich, N., Humler, E., Galois, L., and Bézos, A. (2001) Fe<sup>3+</sup>/ΣFe vs. FeLα peak energy for minerals and glasses: Recent advances with the electron microprobe. *American Mineralogist*, 86(4), 456–465.
- Fialin, M., Bézos, A., Wagner, C., Magnien, V., and Humler, E. (2004) Quantitative electron microprobe analysis of Fe<sup>3+</sup>/ΣFe: Basic concepts and experimental protocol for glasses. *American Mineralogist*, 89(4), 654–662.
- Fialin, M., Wagner, C., and Pascal, M.-L. (2011) Iron speciation using electron microprobe techniques: application to glassy melt pockets within a spinel lherzolite xenolith. *Mineralogical Magazine*, 75(2), 347–362.
- Fischer, D.W. (1965) Changes in the soft X-ray L emission spectra with oxidation of the first series transition metals. *Journal of Applied Physics*, 36(6), 2048–2053.
- Fuchs, P., Almeev, R.R., and Klügel, A. (2014) Experimental constraints on the formation of basanites-phonolite series (Cumbre Vieja, La Palma). *Goldschmidt Abstracts 2014*, 744.
- Gopon, P., Fournelle, J., Sobol, P.E., and Llovet, X. (2013) Low-voltage electron-probe microanalysis of Fe–Si compounds using soft X-rays. *Microscopy and Microanalysis*, 19(6), 1698–1708.
- Höfer, H.E. (2002) Quantification of Fe<sup>2+</sup>/Fe<sup>3+</sup> by electron microprobe analysis—New Developments. In P. Gütllich, B.W. Fitzsimmons, R. Rüfner, and H. Spiering, Eds. *Mössbauer Spectroscopy: Proceedings of the Fifth Seeheim Workshop*, Seeheim, Germany, 21–25 May 2002, p. 239–248. Springer.
- Höfer, H.E., and Brey, G.P. (2007) The iron oxidation state of garnet by electron microprobe: Its determination with the flank method combined with major-element analysis. *American Mineralogist*, 92(5–6), 873–885.
- Höfer, H.E., Brey, G.P., Schulz-Dobrick, B., and Oberhaensli, R. (1994) The determination of the oxidation state of iron by the electron microprobe. *European Journal of Mineralogy*, 6(3), 407–418.
- Höfer, H.E., Weinbruch, S., McCammon, C.A., and Brey, G.P. (2000) Comparison of two electron probe microanalysis techniques to determine ferric iron in synthetic wüstite samples. *European Journal of Mineralogy*, 12(1), 63–71.
- Husen, A., Almeev, R.R., and Holtz, F. (2016) The effect of H<sub>2</sub>O and pressure on multiple saturation and liquid lines of descent in basalt from the Shatsky Rise. *Journal of Petrology*, 57(2), 309–344.
- Jarosewich, E., Nelen, J.A., and Norberg, J.A. (1980) Reference samples for electron microprobe analysis. *Geostandards Newsletter*, 4(1), 43–47.
- Kelley, K.A., and Cottrell, E. (2009) Water and the oxidation state of subduction zone magmas. *Science*, 325, 605–607.
- Kimura, Y., and Akasaka, M. (1999) Estimation of Fe<sup>2+</sup>/Fe<sup>3+</sup> and Mn<sup>2+</sup>/Mn<sup>3+</sup> ratios by Electron Probe Micro Analyzer. *Journal of the Mineralogical Society of Japan*, 28, 159–166.
- Klügel, A., Galipp, K., Hoernle, K., Hauff, F., and Groom, S. (2017) Geochemical and volcanological evolution of La Palma, Canary Islands. *Journal of Petrology*, 58(6), 1227–1248.
- Kress, V., and Carmichael, I. (1991) The compressibility of silicate liquids containing Fe<sub>2</sub>O<sub>3</sub> and the effect of composition, temperature, oxygen fugacity and pressure on their redox states. *Contributions to Mineralogy and Petrology*, 108(1), 82–92.
- Lamb, W.M., Guillemette, R., Popp, R.K., Fritz, S.J., and Chmiel, G.J. (2012) Determination of Fe<sup>3+</sup>/ΣFe using the electron microprobe: A calibration for amphiboles. *American Mineralogist*, 97, 951–961.
- McCammon, C., Chaskar, V., and Richards, G. (1991) A technique for spatially resolved Mössbauer spectroscopy applied to quenched metallurgical slags. *Measurement Science and Technology*, 2(7), 657.
- Moretti, R. (2005) Polymerisation, basicity, oxidation state and their role in ionic modelling of silicate melts. *Annals of Geophysics*, 48, 583–608.
- Morgan, G.B. VI, and London, D. (1996) Optimizing the electron microprobe analysis of hydrous alkali aluminosilicate glasses. *American Mineralogist*, 81, 1176–1185.
- Nikolaev, G.S., Borisov, A.A., and Ariskin, A.A. (1996) Calculation of the ferric-ferrous ratio in magmatic melts: Testing and additional calibration of empirical equations for various magmatic series. *Geochemistry International*, 34, 641–649.
- Potapkin, V., Chumakov, A.I., Smirnov, G.V., Celse, J.-P., Rüfner, R., McCammon, C., and Dubrovinsky, L. (2012) The <sup>57</sup>Fe synchrotron Mössbauer source at the ESRF. *Journal of Synchrotron Radiation*, 19, 559–569.
- Pouchou, J.L., and Pichoir, F. (1991) Quantitative analysis of homogeneous or stratified microvolumes applying the model “PAP”. In K.F.J. Heinrich and D.E. Newbury, Eds., *Electron Probe Quantitation*, p. 31–75. Plenum Press, New York.
- Sack, R., Carmichael, I., Rivers, M., and Ghiorso, M. (1981) Ferric-ferrous equilibria in natural silicate liquids at 1 bar. *Contributions to Mineralogy and Petrology*, 75(4), 369–376.
- Savitzky, A., and Golay, M.J.E. (1964) Smoothing and differentiation of data by simplified least squares procedures. *Analytical Chemistry*, 36(8), 1627–1639.
- Schuessler, J.A., Botcharnikov, R.E., Behrens, H., Misiit, V., and Freda, C. (2008) Oxidation state of iron in hydrous phono-tephritic melts. *American Mineralogist*, 93, 1493–1504.
- Shishkina, T., Botcharnikov, R., Holtz, F., Almeev, R.R., and Portnyagin, M. (2010) Solubility of H<sub>2</sub>O and CO<sub>2</sub>-bearing fluids in tholeiitic basalts at pressures up to 500 MPa. *Chemical Geology*, 277, 115–125.
- Tossell, J., Vaughan, D., and Johnson, K. (1974) Electronic-structure of rutile, wüstite, and hematite from molecular-orbital calculations. *American Mineralogist*, 59, 319–334.
- van Aken, P.A., and Liebscher, B. (2002) Quantification of ferrous/ferric ratios in minerals: New evaluation schemes of Fe L 23 electron energy-loss near-edge spectra. *Physics and Chemistry of Minerals*, 29, 188–200.
- van Aken, P., Liebscher, B., and Styrsky, V. (1998) Quantitative determination of iron oxidation states in minerals using Fe L<sub>2,3</sub>-edge electron energy-loss near-edge structure spectroscopy. *Physics and Chemistry of Minerals*, 25(5), 323–327.
- Wilke, M. (2005) Fe in magma—An overview. *Annals of Geophysics*, 48(4–5), 609–617.
- Wilke, M., Behrens, H., Burkhard, D.J., and Rossano, S. (2002) The oxidation state of iron in silicic melt at 500 MPa water pressure. *Chemical Geology*, 189(1), 55–67.
- Wilke, M., Farges, F., Partzsch, G.M., Schmidt, C., and Behrens, H. (2007) Speciation of Fe in silicate glasses and melts by in-situ XANES spectroscopy. *American Mineralogist*, 92, 44–56.
- Wilson, A. (1960) The micro-determination of ferrous iron in silicate minerals by a volumetric and a colorimetric method. *Analyst*, 85(1016), 823–827.
- Zhang, C., Koepke, J., Wang, L.-X., Wolff, P.E., Wilke, S., Stechern, A., Almeev, R., and Holtz, F. (2016) A practical method for accurate measurement of trace level fluorine in Mg- and Fe-bearing minerals and glasses using electron probe microanalysis. *Geostandards and Geoanalytical Research*, 40(3), 351–363.

MANUSCRIPT RECEIVED DECEMBER 17, 2017

MANUSCRIPT ACCEPTED APRIL 27, 2018

MANUSCRIPT HANDLED BY MAURIZIO PETRELLI

### Endnote:

<sup>1</sup>Deposit item AM-18-96437, Supplemental Material. Deposit items are free to all readers and found on the MSA web site, via the specific issue's Table of Contents (go to [http://www.minsocam.org/MSA/AmMin/TOC/2018/Sep2018\\_data/Sep2018\\_data.html](http://www.minsocam.org/MSA/AmMin/TOC/2018/Sep2018_data/Sep2018_data.html)).